physica status solidi pss a
www.pss-a.com

Nanoporous Ag Films Prepared by Cluster-Source Sputtering as Substrates for Surface-Enhanced Raman Scattering

Sungho Yun, Junyeop Lee, Jaemoon Yang, Dongin Lee, Bonghwan Kim, and Chanseob Cho**

By mounting a cluster source on a conventional sputtering system, a new sputtering system is devised for the deposition of nanoporous metal thin films at room temperature. First, the diameter of the nozzle is fixed while the pressure inside the cluster source is kept at several hundreds of mTorr. By adjusting the length of the cluster source, nanoporous films of different thickness can be formed at room temperature. The Raman response characteristics according to the process conditions are then analyzed, and the applicability of the sputtered thin film as a substrate for surface-enhanced Raman scattering (SERS) is examined. The results show that the Raman intensity increases with increasing film thickness and reaches a saturated value at a thickness of 2 μm. Therefore, the proposed system takes advantage of an existing sputtering process, and it is possible to form a nanoporous metal film with thickness of several micrometers or more that can be used as a Raman substrate.

1. Introduction

Various fields such as sterilization of biological agents and gas sensing have seen major advances owing to the development of synthesis technology for nanomaterials like gold and silver, which have been used for decorative, wiring, and catalyst applications.[1–4] It was recently discovered that nanoparticles consisting of noble metals like gold and silver can strongly resonate with light in the visible range; since then, there has been active research on this property.[5] In particular, the phenomenon of surface plasmon resonance (SPR) of nanoparticles is actively applied to Raman spectroscopy as well as DNA identification.[6–8]

Raman spectroscopy allows the molecular structure of a material to be estimated by measuring the vibrational energy of certain functional groups present in the sample. Application of the technique was limited in the early days because of the low probability of Raman scattering of molecules and the possibility of strong background fluorescence.[9,10] Since the phenomenon of surface-enhanced Raman scattering (SERS) using silver electrodes was discovered, however, this spectroscopic method has been widely used as a powerful analysis tool.[11]

Localized surface plasmon resonance (LSPR), which is observed in nanoparticles of noble metals such as gold and silver, is a phenomenon in which SPR is concentrated in fine particles without spreading throughout the particles or structure.[12–14] LSPR is a major means of obtaining sensitive responses to the adsorption and reaction of a substance on a metal surface.

The main materials that can be used as LSPR sensors are gold, silver, and aluminum. Gold is used for biological experiments because of its high biocompatibility and stability[15]; the biocompatibility and stability of silver and aluminum are low, but the sensitivity of a sensor made of silver or aluminum is high because of its optical properties. The purpose of this study is to fabricate a substrate for SERS-based biosensors based on SERS, so silver nanoparticles were used to form the metal nanostructures examined in this experiment.[6,7,9,10]

Resonance occurs when the frequency of incident light and the frequency of collective motion of surface plasmons are the

S. Yun, J. Lee, Prof. C. Cho
School of Electronics Engineering
Kyungpook National University
Daegu 41566, Korea
E-mail: chocs@knu.ac.kr

Dr. S. Yun
Kwang-Lim Precision, Inc.
Daegu 43013, Korea

Prof. J. Yang
Yonsei University
Seoul 03722, Korea

Prof. D. Lee
Department of Information and Communication Engineering
Yeungnam University
Gyeogbuk 38541, Korea

Prof. B. Kim
School of Electronics and Electrical Engineering
Daegu Catholic University
Gyeongbuk 38430, Korea
E-mail: bhkim@cu.ac.kr

The ORCID identification number(s) for the author(s) of this article can be found under https://doi.org/10.1002/pssa.201701010.

DOI: 10.1002/pssa.201701010

same. When noble-metal nanostructures such as those of Au and Ag exhibit resonance, the electromagnetic field induced by the surface plasmons amplifies the Raman signal of the adsorbed material.[16] Therefore, the most important component in a SERS-based biosensor is the substrate on which the metal nanostructure is formed.[17–19] Although a substrate can exhibit a high SERS enhancement factor (EF), it is difficult to control the substrate to ensure signal homogeneity and grain stability. Therefore, it is impossible to widely apply SERS to large-area sensing.[20,21] Among the methods of thin-film deposition based on a semiconductor process, sputtering can be used to deposit various materials such as metals, compounds, and insulators; it also has the advantages of adaptability to large-scale production, uniform film growth, and excellent step coverage.

Ag-based SERS substrates have the disadvantage of poor chemical stability.[22] Qui et al.[23] reported the fabrication of a flexible SERS substrate consisting of graphene/Ag-nanoflowers/PMMA. Yang et al.[24] prepared an inverted nanotaper-based Ag film that was conveniently fabricated by thermal evaporation of Ag nanoparticles on a tapered PAA structure, which served as the substrate. Ouyang et al.[25] demonstrated a reusable SERS sensor based on a laser-wrapped graphene–Ag array.

In this study, a sputtering system equipped with a cluster source was designed for the formation of nanoclusters at room temperature.[26–31] The formation characteristics of the nanoporous structures were determined for different values of system pressure, process temperature, and He feeding ratio. We then compared these formation characteristics to investigate the possibility of using the system to produce large-scale SERS substrates.

2. Design of Sputtering System

We designed a sputtering system equipped with a cluster source, as shown in **Figure 1**, for the formation of nanoporous Ag metal films. This device consisted of a main chamber (process chamber) and a cluster-source section, in which a nanocluster was generated and transported to the main process chamber.

The cluster-source section consisted of the following four parts: 1) a direct-current (DC) magnetron sputtering unit that used Ar-ion sputtering to form particles from a target; 2) the condensation (or aggregation) region (labeled by the dimension *d* in Figure 1) in which nanoclusters were formed by nucleation of neighboring particles as they moved toward the main deposition chamber while being cooled; 3) the nozzle (aperture) served as a channel for the nanoclusters to enter the main deposition chamber; 4) a water-cooling system to cool the condensation zone. The process chamber, which was the region where the nanoclusters from the cluster source reached the substrate, was designed to control the process pressure, independent of the cluster source.

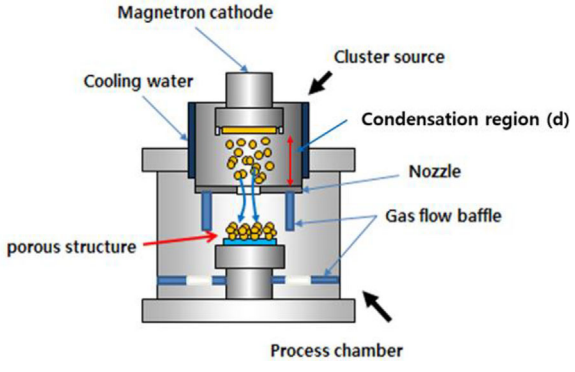

Figure 1. Schematic diagram of cluster source sputter system.

The metal particles sputtered by Ar ions were cooled as they passed through the condensation region of the cluster source; the cooled metal particles then nucleated with adjacent particles to form nanoclusters. The pressure inside the cluster source was determined by the aperture size and the gas (Ar, He, etc.) injected into the cluster source. To increase the nucleation of the particles generated by Ar sputtering and to allow the formation of nanoclusters at room temperature, the pressure inside the cluster source should be maintained at several hundreds of millitorr. In this study, the diameter of the nozzle was designed to be 40 mm. In addition, the length (*d*) of the cluster source was designed to be adjustable from 139 to 214 mm in order to characterize the nanoporous thin-film formation according to the length of the condensation region.

3. Experimental Method and Sample Preparation

The deposition rate and film properties of the nanoporous metal structure were determined by the length of the condensation region, the pressure of the condensation region, the aggregate gas flow rate, and the pressure of the process chamber. The basic conditions of the experiment were a DC power of 140 W, cluster-source pressure of 440 mTorr, process-chamber pressure of 200 mTorr, process temperature of 15 °C, He concentration of 17.6%, and condensation-region length of 164 mm. During the experiment, the total gas flow rate was fixed at 100 $cm^3\,min^{-1}$. As the experiment progressed, the process chamber pressure, cluster source temperature, and He ratio were changed systematically to determine the nanoporous-structure formation characteristics. The optimal process conditions were determined through several preliminary experiments.

The porosity of thin films is usually determined using gravimetric or quasi-gravimetric methods.[28,29,32,33]

Porosity is defined as the fraction of the bulk sample volume (V) that is not occupied by solid matter.[28,29] In this study, we measured the porosity using the gravimetric method based on the following relationship:

$$\text{Porosity} = \frac{M_1 - M_2}{M_1} \tag{1}$$

where M_2 is the weight of the deposited nanoporous film (difference between the weight of the target before and after sputtering), and M_1 is the weight of the bulk Ag film, whose thickness was the same as that of the nanoporous film.

In order to investigate whether a metallic Ag substrate with nanoporous structure fabricated using the newly designed sputtering system can be used as a SERS-based biosensor

substrate, the Raman response characteristics were measured with a Rhodamine 6G (R6G) solution to evaluate the performance of the biosensor. A schematic diagram of the sample preparation process for SERS measurements is shown as **Figure 2**. First, a Ag nanoporous film was vapor-deposited on a $10 \times 10\,mm^2$ square Si substrate under various conditions by cluster sputtering of a target. Next, 1 μL (1×10^{-9} mol) of an aqueous 1 mM R6G solution was released in droplets at the center and four corners of the substrate using a micropipette, and the droplets were left to dry at room temperature for 20 min. Finally, Raman measurements were recorded three times at each point on the R6G/Ag/Si system, and the average value was obtained after 15 measurements were taken on each sample. The laser wavelength and output power of the Raman system (QEPRO, Oceanoptics, USA) used in the measurements were 785 nm and 15 mW, respectively.

The enhancement factor is generally used as an indicator of the performance of a SERS substrate, and it is defined by Equation (2) as follows[34]:

$$EF = \frac{I_{SERS}}{I_R}\frac{C_R}{C_{SERS}} \tag{2}$$

where I_R and C_R are the Raman signal intensity and concentration, respectively, of the molecules in the R6G solution when there was no SERS substrate, and I_{SERS} and C_{SERS} are the Raman signal intensity and the molecular concentration, respectively, of the R6G solution measured on the SERS substrate. The concentration of R6G was $C_R = 2 \times 10^{-5}$ mol ($1\,mM \times 20\,mL = 2 \times 10^{-5}$ mol) when measured in the aqueous solution and $C_{SERS} = 1 \times 10^{-9}$ mol ($1\,mM \times 1\,\mu L = 1 \times 10^{-9}$ mol) when measured on the SERS substrate.

X-ray diffraction (XRD) patterns of the samples prepared at chamber pressures of 50 and 200 mTorr were recorded with a powder diffractometer (Pro-MPD, PANalytical, the Netherlands) in the 2θ range of 30–70°.

4. Results and Discussion

4.1. Analysis of Thickness of Ag Nanoporous Thin Films and Raman Response Characteristics

To analyze the change in thickness of the sputtered film, the length of the condensation region (the distance between the target and the nozzle) was fixed at 164 mm, and the aggregate gas flow rate into the cluster source chamber was maintained at a constant value of $100\,cm^3\,min^{-1}$ ($85\,cm^3\,min^{-1}$ for Ar, $15\,cm^3\,min^{-1}$ for He). Next, a Ag nanoporous thin film with a specific thickness was deposited by controlling the process duration while keeping the process pressure of the cluster source chamber constant at 440 mTorr and the process chamber constant at 200 mTorr. The required process duration was obtained from several preliminary experiments. **Figure 3**(a) and (b) show cross-sectional and surface SEM images and Raman responses, respectively, of the Ag nanoporous films deposited by cluster sputtering. Regardless of the thickness, the surface and cross section of the deposited thin film were uniform and displayed a constant porosity. As shown in the images, the films with thickness of 0.83 and 2.35 μm had the same porosity of 79.2%. From this result, we found that the porosity was constant regardless of the growth time of the thin film. In other words, even though the film thickness increased with longer process time, the Ag clusters deposited on the surface of the thin film remained at a constant size of 40–50 nm. The phenomenon can be explained as follows. First, Ag clusters generated in the condensation region of the sputtering system were transferred to the substrate in the process chamber and adsorbed on the

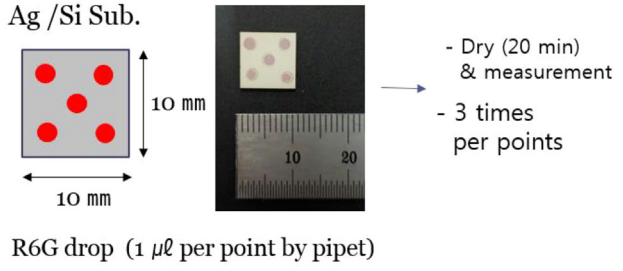

Figure 2. Sample preparation for SERS measurement.

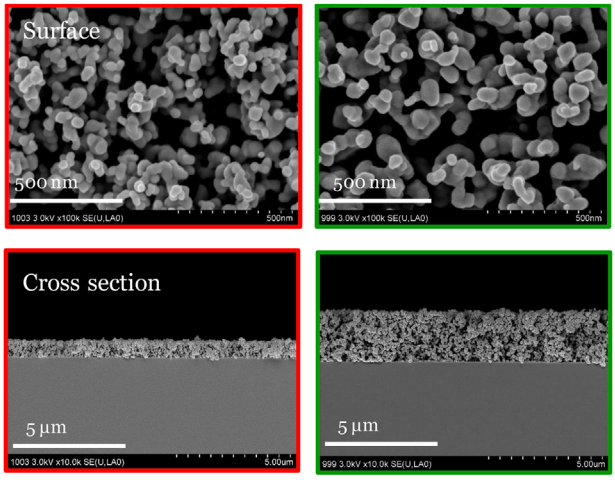

(a)

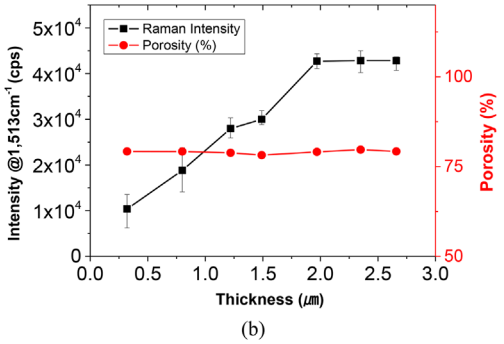

(b)

Figure 3. a) Surface and cross-sectional SEM images and (b) Raman response and porosity with thickness of the Ag nanoporous thin film.

substrate to form island structures with dimensions of several tens of nanometers. These structures were deposited and adsorbed in the vertical direction while maintaining a gap in the horizontal direction to grow a thin film with a porous structure.

Next, the Raman response characteristics of the substrate with an overlying Ag nanoporous metal structure fabricated by cluster-source sputtering were measured as a function of the film thickness. The Raman response characteristics of an aqueous 1 mM R6G solution were also investigated to check its applicability as a Raman measurement substrate for biosensors. The Raman measurements on the Ag nanoporous substrate were performed by releasing 1 μL (1×10^{-9} mol) of the aqueous 1 mM R6G solution in droplets onto a 1×1 mm^2 region. After a total volume of 20 mL of the R6G solution was released onto the Ag substrate, almost no Raman signal was detected in the entire frequency range. However, a very large Raman signal was detected on the Ag nanoporous substrate, especially at the wavenumber of 1514 cm^{-1}, where the signal intensity was at a maximum. The Raman intensity was 1×10^4 cps when the thickness of the thin film was 0.32 μm, and it increased with the thickness of the thin film. When the film thickness exceeded 2 μm, the Raman intensity showed a similar value of about 4.3×10^4 cps. In general, an increase in film thickness increases the number of hot spots that can amplify the Raman signal; however, when the film thickness reaches a threshold, the effective hot spot region capable of reacting with the solution becomes saturated. Therefore, it is believed that the R6G molecules did not invade the deep hot spots far from the surface, and they did not participate in Raman-signal amplification. It can be seen in Figure 3 that the maximum penetration depth of R6G molecules in a Ag nanoporous film with porosity of 78–79% was about 2 μm.

Thus, in the experiments, according to the subsequent formation condition of nanoporous Ag thin films, the Raman response characteristics were measured by controlling the deposition time under individual deposition conditions by growing the Ag nanoporous film at 2 μm.

The standard deviation of the Raman signal intensity measured at the center and four corners of the 10×10 mm^2 specimen was 25% at 0.4 μm. However, the standard deviation decreased as the thickness of the thin film increased: when the film thickness was over 2 μm, the standard deviation was less than 2.5%. Therefore, we conclude that a nanoporous Ag thin film fabricated by cluster-source sputtering is suitable for the fabrication of large-scale Raman substrates.

4.2. Analysis of Thin-Film Formation Characteristics According to Process-Chamber Pressure

The vacuum valve of the process chamber was adjusted to vary the process pressure between 50 and 350 mTorr, and other process conditions remained the same to focus on the effect of the process pressure. During the experiment, the total amount of gas entering the cluster-source chamber was kept constant at 100 cm^3 min^{-1}. The thickness of the deposited Ag film was adjusted to 2 μm, which was the thickness at which the Raman intensity became saturated by controlling the process duration. **Figure 4** shows SEM images of the surface films produced at various values of the process chamber pressure. It can be seen that the nanoporous metal structure was uniformly formed on the silicon substrate, even though the process pressure varied from 50 to 350 mTorr. As the process pressure increased, the distance between the metal clusters also increased and a more porous metal structure was formed; however, the deposition rate decreased as the process pressure was increased. The porosity increased because of the increase in condensation owing to the decrease in cluster velocity in the cluster source, the decrease in mean free path of the clusters in the substrate, and the decrease in deposition rate. The deposition rate decreased because the particle velocity decreased owing to the decrease in pressure difference between the cluster source and the process chamber, and the decrease in difference in the mean free path of the particles with changing pressure conditions inside the process chamber, while the pressure of the process chamber increased under constant pressure inside the cluster source.

Figure 5 shows the XRD patterns of the Ag nanoporous films prepared when the chamber pressure was 50 and 200 mTorr. The patterns do not indicate the presence of impurities such as Ag_2O on the film. The main diffraction peaks of the Ag nanoporous films were recorded at 38.061, 44.061, and 64.408°, which correspond to the (111), (200), and (220) planes, respectively, of face-centered cubic (fcc) silver. The XRD intensity did not vary significantly with the chamber pressure utilized for film formation. The ratio of intensity between the (111) and (200) peaks has values of 4.1 for both films prepared at 50 and 200 mTorr, indicating that the nanoporous film had an abundance of (111) facets.

Figure 6 shows the Raman intensity, EF, and porosity as functions of the process-chamber pressure. The value of EF was calculated using Equation (1), and the Raman intensity was

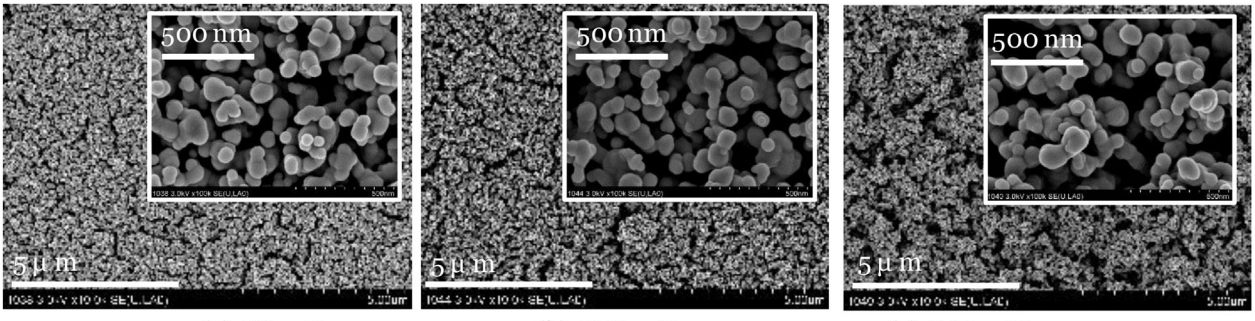

Figure 4. SEM pictures according to process chamber pressure.

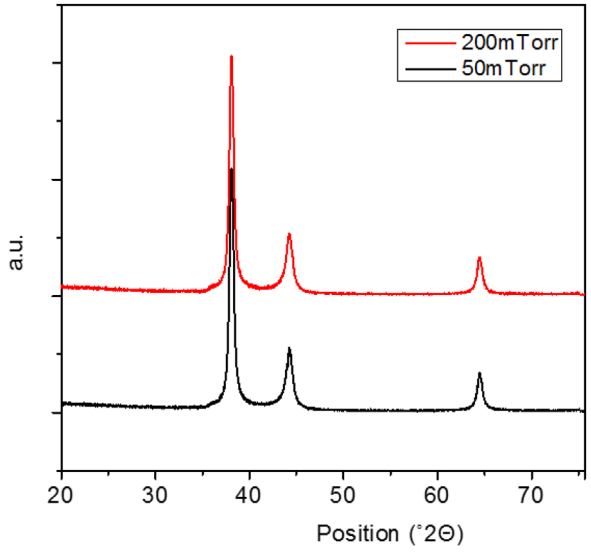

Figure 5. XRD pattern of Ag nanoporous film with process chamber pressure.

measured at 1514 cm^{-1}, the wavenumber at which the maximum peak was observed. As the process pressure increased, the Raman intensity and porosity increased, and EF also increased from 3.21×10^6 at 50 mTorr to 5.7×10^6 at 350 mTorr because the increase in hot spots amplified the Raman signal, and the easier penetration of R6G molecules owing to the increased gap and porosity among the clusters as the pressure of the process chamber increased. Therefore, in order to prepare a SERS substrate with high sensitivity, it was necessary to increase the porosity of the nanoporous Ag thin film. The process pressure of 350 mTorr in this study was the maximum pressure that could be controlled by the equipment used in the experiment.

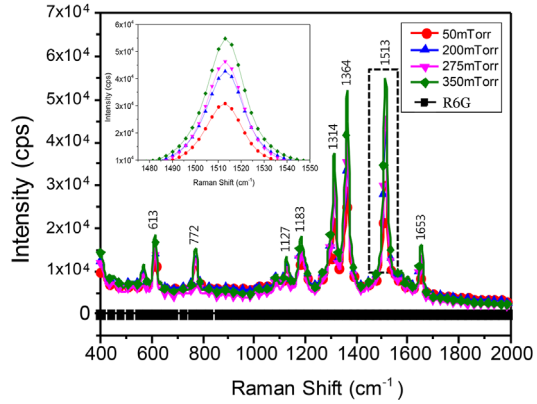

Process Condition	50mT	200mT	275mT	350mT
Porosity (%)	70.7	79.1	80.2	81.0
EF	3.21×10^6	4.44×10^6	4.82×10^6	5.70×10^6

Figure 6. Raman response and its porosity by process chamber pressure.

The shape of the thin film was observed by scanning electron microscopy (SEM) to investigate the cause of increase in porosity with process pressure. In the early stage of the process, the lower the process chamber pressure, the higher the density of the clusters deposited on the Si substrate. As the deposition duration increased, the clusters on the surface became denser. When the deposition duration was further increased, the porous thin film grew while maintaining the initial deposited shape. A thin film formed under general sputtering conditions follows the Volmer–Weber film formation mechanism, which is described as follows: a three-dimensional core first forms on the substrate surface; the core then forms an island casting; finally, the island structures connect. On the other hand, the growth of a nanoporous thin film by cluster-source sputtering is based on the adjacent clusters agglomerating with each other while maintaining the gap between them instead of growing in the horizontal direction. In our system, as the generated clusters in the cluster source moved toward the substrate via the nozzle, they became adsorbed by the substrate, thereby forming a thin film with nanoporous structure. The experiment shows that the working pressure had a significant effect on the initial distribution of clusters. In addition, the porosity and deposition rate were the key variables affecting the properties of the deposited thin films.

4.3. Analysis of Thin-Film Formation Characteristics According to Length of Condensation Region

When the length of the condensation region was increased, the cluster size of the deposited films slightly increased. The porosity increased from 73% at a length of 139 mm to 79% at 175 mm, but it slightly decreased to 77% at 214 mm. **Figure 7** explains how the increase in porosity led to the formation and deposition of large clusters on the substrate.

The thickness of the deposited Ag nanoporous film was ≈2 μm, in which the Raman intensity was saturated.

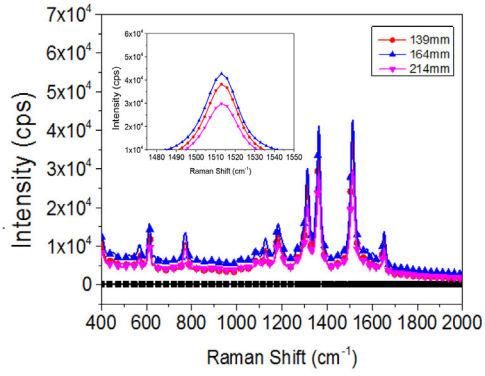

Process Condition	139mm	164mm	214mm
Porosity (%)	73.9	79.1	77.1
EF	3.97×10^6	4.44×10^6	3.06×10^6

Figure 7. Raman response and its porosity with length of the condensation region.

The Raman response was reduced to 3.97×10^6 and 3.06×10^6 at 135 and 214 mm, respectively, and the EF was 4.44×10^6 at 175 mm. When the length of the condensation region was 135 mm, the smaller clusters aggregated on the substrate surface to form clusters of larger sizes, but the hot-spot density decreased. Because of that, the penetration depth of the R6G molecules was reduced. When the length of the condensation region was 214 nm, the porosity slightly decreased and the hot-spot density was also decreased owing to the increased cluster size. These results confirm that the cluster size and porosity of the nanoporous thin film was affected by the length of the condensation region. We think it is necessary to carry out further analysis of the nanoporous-film-formation characteristics by increasing the rate of change in the condensation-region length.

4.4. Analysis of Thin-Film Formation Characteristics According to Temperature of Cluster Source

The cluster size remained almost constant because of the small effect of the narrow temperature range and the short cluster source (condensation region), although the increase in nucleation caused a decrease in deposition rate at lower temperatures. The thickness of the Ag nanoporous film was adjusted to ≈2 μm, in which the Raman intensity was saturated by adjusting the deposition time.

When the temperature of the cluster source was 5 °C, the porosity of the deposited thin film was 78.7%, and it slightly increased to 79.4% when the film was prepared with a cluster-source temperature of 10 °C. The porosity tended to decrease with increasing deposition temperature, reaching 78.6% for the film deposited with a cluster-source temperature of 20 °C. For the Raman response, EF increased from 3.52×10^6 for the film deposited with a cluster-source temperature of 5 °C to 4.4×10^6 for the film deposited with a cluster-source temperature below 20 °C. However, as shown in **Figure 8**, EF decreased to 3.52×10^6 for the film prepared with a cluster-source temperature of 20 °C.

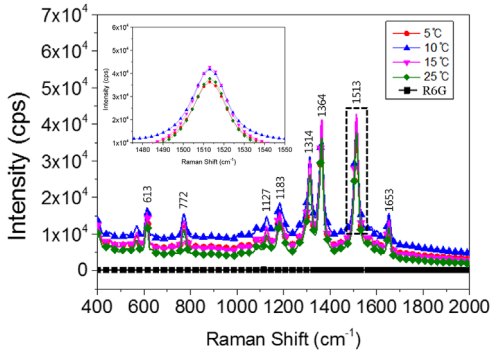

Process Condition	5°C	10°C	15°C	20°C
Porosity (%)	78.7	79.4	79.1	78.6
EF	3.52×10^6	4.35×10^6	4.44×10^6	3.92×10^6

Figure 8. Raman response and its porosity by temperature.

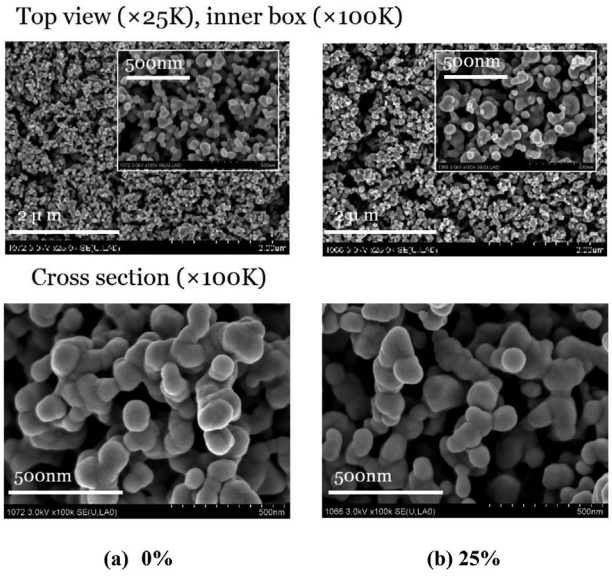

Figure 9. SEM pictures according to He ratio.

As the temperature of the cluster-source increased, the thin-film deposition rate slightly decreased. It can be seen that a large temperature range is required to study the characteristics of thin-film formation and the Raman response as functions of temperature of the cluster source.

4.5. Analysis of Thin-Film Formation Characteristics According to Ratio of He

The images in **Figure 9** show the formation of thin films at He input ratios of 0 and 25%. As shown in **Figure 10**, a uniform

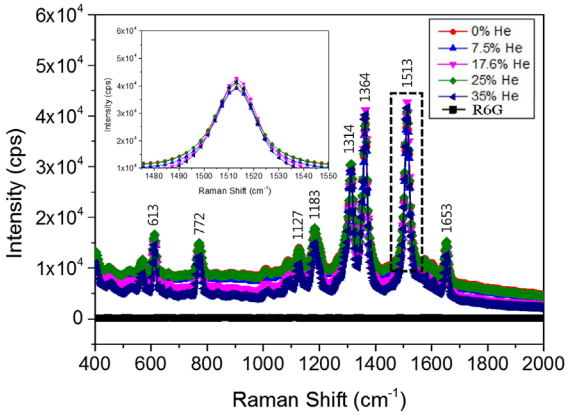

Process Condition	0% He	7.5% He	17.6% He	25% He	35% He
Porosity (%)	77.7	77.4	79.1	79.3	74.3
EF	4.09×10^6	4.06×10^6	4.44×10^6	4.25×10^6	4.33×10^6

Figure 10. Raman response and its porosity by He ratio.

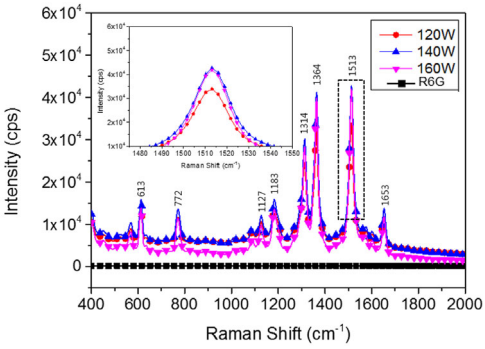

Process Condition	120W	140W	160W
Porosity (%)	72.6	79.1	77.1
EF	3.54×10^{6}	4.44×10^{6}	4.36×10^{6}

Figure 11. Raman response and its porosity by power.

nanoporous metal structure was formed regardless of the ratio of He. Here, the thickness of the sample was adjusted to ≈2 μm, in which the Raman intensity was saturated by controlling the deposition time.

The EF in Raman response was 4.06×10^6 when the relative partial pressure of He was 7.5%; it increased to 4.4×10^6 when the relative partial pressure of He was increased to 17.6%, but it decreased when the relative partial pressure of He was further increased. As the He ratio increased, the crystal size decreased, but the deposition rate increased. Since the viscosity of He is lower than that of Ar, the deposition rate increased as the concentration of He increased. In addition, as the partial pressure of He increased, the viscosity of the entire gas mixture decreased; the crystal size decreased as well because the particles condensed in the cluster source and moved to the process chamber before they became larger. The porosity continued to increase up to a He ratio of 25% because of the increase in deposition rate with the increase in low partial pressure of He, but it decreased at a He ratio of 35% because of the effect of the reduced crystal size.

4.6. Analysis of Thin-Film Formation Characteristics According to DC Power

Figure 11 shows the Raman response and porosity of the thin film as functions of the supplied power. The thickness of the Ag nanoporous film was adjusted to ≈2 μm by adjusting the deposition time. We observed that EF was 3.54×10^6 when the power was 120 W, and it increased to 4.44×10^6 when the power was 140 W. However, it decreased when the power was 160 W.

5. Conclusion

We devised a sputtering system for depositing nanoporous metal thin films at room temperature by using a cluster source in a conventional sputter system. This approach is advantageous because it utilizes an existing sputtering process. The surfaces and cross sections of the deposited films were uniform, and the porosity remained constant regardless of the deposition duration. Even though the deposited Ag clusters increased in thickness as the process duration was increased, the clusters remained at a constant size of 40–50 nm.

The Raman response characteristics of the resulting thin film were analyzed as the process conditions were varied. The Raman intensity increased as the thickness of the thin film increased. The Raman intensity reached a saturated value of 4.3×10^4 cps when the film thickness was about 2 μm. We confirmed that a nanoporous metal structure was uniformly formed on the silicon substrate even when the process pressure was varied between 50 and 350 mTorr. The Raman intensity and porosity increased with increasing process pressure. The working pressure had a large impact on the initial cluster distribution. In addition, the deposition rate and porosity were the main variables that affected the properties of the thin film. The Raman response depended on the porosity of the nanoporous metal, and it had a tendency to reach a saturated value when the film thickness was over 2 μm.

Most important of all, we confirmed that it is possible to use the cluster-source sputtering system to form a thick nanoporous metal film with a thickness of several micrometers or more.

Acknowledgments

This research was supported by the Basic Science Research Program through the National Research Foundation of Korea (NRF) funded by the Ministry of Education (NRF-2017R1D1A3B03034258); the Basic Science Research Program through the National Research Foundation of Korea (NRF) funded by the Ministry of Education (No. NRF-2016R1D1A3A03919627); and the Ministry of Science, ICT and Future Planning (MSIP), Korea, under the Information Technology Research Center (ITRC) support program (IITP-2018-2016-0-00313) supervised by the Institute for Information & communications Technology Promotion (IITP). This research was also supported by the Technological innovation R&D program of SMBA [S2448674].

Conflict of Interest

The authors declare no conflict of interest.

Keywords

biosensors, cluster source, nanoporous, surface-enhanced Raman scattering

Received: December 9, 2017
Revised: May 26, 2018
Published online:

[1] D. V. Talapin, J. S. Lee, M. V. Kovalenko, E. V. Shevchenko, *Chem. Rev.* **2010**, *110*, 389.
[2] C. Burda, X. Chen, R. Narayanan, M. A. El-Sayed, *Chem. Rev.* **2005**, *105*, 1025.
[3] Y. Xia, Y. Xiong, B. Lim, S. E. Skrabalak, *Angew. Chem. Int. Ed. Engl.* **2009**, *48*, 60.
[4] J. Zhang, C. M. Li, *Chem. Soc. Rev.* **2012**, *41*, 7016.

[5] K. Kneipp, M. Moskovits, H. Kneipp, *Surface-Enhanced Raman Scattering: Physics and Applications*, Vol. 103, Springer, Atlanta **2006**.
[6] D. K. Lim, K. S. Jeon, J. H. Hwang, H. Kim, S. Kwon, Y. D. Suh, J. M. Nam, *Nat. Nanotechnol*. **2011**, *6*, 452.
[7] Z. Wang, L. Tang, L. H. Tan, J. Li, Y. Lu, *Angew. Chem. Int. Ed Engl*. **2012**, *51*, 9078.
[8] J. Lee, B. Hua, S. Park, M. Ha, Y. Lee, Z. Fan, H. Ko, *Nanoscale* **2014**, *6*, 616.
[9] A. Otto, I. Mrozek, H. Grabhorn, W. Akemann, *J. Phys.: Condens. Matter* **1992**, *4*, 1143.
[10] C. L. Haynes, A. D. McFarland, R. P. Van Duyne, *Anal. Chem*. **2005**, *77*, 338-A.
[11] M. Fleischmann, P. J. Hendra, A. J. McQuillan, *Chem. Phys. Lett*. **1974**, *26*, 163.
[12] F. Beck, S. Mokkapati, A. Polman, K. Catchpole, *Appl. Phys. Lett*. **2010**, *96*, 033113.
[13] C. Hägglund, M. Zäch, B. Kasemo, *Appl. Phys. Lett*. **2008**, *92*, 013113.
[14] M. D. Brown, T. Suteewong, R. S. S. Kumar, V. D'Innocenzo, A. Petrozza, M. M. Lee, U. Wiesner, H. J. Snaith, *Nano Lett*. **2010**, *11*, 438.
[15] H. Jans, Q. Huo, *Chem. Soc. Rev*. **2012**, *41*, 2849.
[16] S. A. Maier, *Plasmonics: Fundamentals and Applications*. Springer, Atlanta **2007**.
[17] J. Stropp, G. Trachta, G. Brehm, S. Schneider, *J. Raman Spectrosc*. **2003**, *34*, 26.
[18] J. F. Li, Y. F. Huang, Y. Ding, Z. L. Yang, S. B. Li, X. S. Zhou, F. R Fan, W. Zhang, Z. Y. Zhou, B. Ren, Z. L. Wang, *Nature* **2010**, *464*, 392.
[19] W. C. Lin, L. S. Liao, Y. H. Chen, H. C. Chang, D. P. Tsai, H. P. Chiang, *Plasmonics* **2011**, *6*, 201.
[20] E. D. Diebold, N. H. Mack, S. K. Doorn, E. Mazur, *Langmuir* **2009**, *25*, 1790.
[21] J. Fontana, J. Livenere, F. J. Bezares, J. D. Caldwell, R. Rendell, B. R. Ratna, *Appl. Phys. Lett*. **2013**, *102*, 201606.
[22] K. C. Bantz, A. F. Meyer, N. J. Wittenberg, H. Imb, Ö. Kurtuluş, S. H. Lee, N. C. Lindquist, S.-H. Oh, C. L. Haynes, *Phys. Chem. Chem. Phys*. **2011**, *13*, 11551.
[23] H. Qiu, M. Wang, S. Jiang, L. Zhang, Z. Yang, L. Li, J. Li, M. Cao, J. Huang, *Sens. Actuat. B* **2017**, *249*, 437.
[24] C. Yang, Y. Qin, X. Zhu, M. Yin, D. Li, X. Chen, Y. Song, *J. Alloys Compd*. **2015**, *632*, 634.
[25] L. Ouyang, Y. Hu, L. Zhu, G. J. Cheng, J. Irudayaraj, *Biosens. Bioelectron*. **2017**, *92*, 755.
[26] K. Wegner, P. Piseri, H. V. Tafreshi, P. Milani, *J. Phys. D: Appl. Phys*. **2006**, *39*, R439.
[27] A. N. Banerjee, R. Krishna, B. Das, *Appl. Phys. A* **2008**, *90*, 299.
[28] C. Flagan, M. M. Lunden, *Mater. Sci. Eng*. **1995**, *A204*, 113.
[29] H. Haberland, M. Mall, M. Moseler, Y. Qiang, T. Reiners, Y. Thurner, *Vac. Sci. Technol. A* **1994**, *12*, 2925.
[30] V. Singh, P. Grammatikopoulos, C. Cassidy, M. Benelmekki, M. Bohra, Z. Hawash, K. W. Baughman, M. Sowwan, *J. Nanopart. Res*. **2014**, *16*, 2373.
[31] M. T. Swihart, *Curr. Opin. Colloid Interface Sci*. **2003**, *8*, 127.
[32] R. Herino, G. Bomchil, K. Barla, C. Bertrand, *J. Electrochem. Soc*. **1987**, *134*, 1994.
[33] J. Peckham, G. T. Andrews, *Thin Solid Films* **2012**, *520*, 2526.
[34] H. M. Lee, S. M. Jin, H. M. Kim, Y. D. Suh, *Phys. Chem. Chem. Phys*. **2013**, *15*, 5276.